




12.1%


Not yet Date: 2022-10-23 05:15 UTC


* All sources 100 Internet sources 18 Publisher sources 6 Organization archive 5 Plagiarism Prevention Pool 23


- [0]  www.science.gov/topicpages/g/galapagos+mantle+plume
9.3% 48 matches


- [1]  www.researchgate.net/publication/252094290_Mantle_Flow_beneath_Arabia_Offset_from_the_Opening_Red_Sea
4.1% 44 matches


- [3]  www.researchgate.net/publication/267415548_Seismic_Structure_of_the_Arabian_Shield_Lithosphere_and_Red_Sea_Margin
4.1% 42 matches


- [8]  www.sciencedirect.com/science/article/abs/pii/S1367912016300190
2.4% 32 matches


- [11]  www.researchgate.net/publication/221922192_Multiscale_Seismic_Tomography_Imaging_of_Volcanic_Complexes
2.2% 20 matches


- [14]  www.solid-earth.net/5/873/2014/
0.7% 14 matches
1 documents with identical matches


- [18]  from a PlagScan document dated 2018-05-28 06:39
0.6% 7 matches


- [19]  "DIIT Magnetic Manuscript.docx" dated 2022-07-26
0.1% 8 matches


- [20]  Incipient status of dyke intrusion in top crust – evidences from the Al-Ays 2009 earthquake swarm, Harrat Lunayyir, SW Saudi Arabia
0.2% 6 matches


- [21]  Structure of the Tasmanian lithosphere from 3D seismic tomography
0.2% 7 matches


- [23]  academic.oup.com/gji/article/188/3/1173/685895
0.0% 8 matches


- [24]  "2-17-01-001-0016.pdf" dated 2017-06-08
0.5% 4 matches


- [25]  Seismic wave attenuation beneath the Australasian region
0.1% 6 matches


- [26]  from a PlagScan document dated 2021-11-01 10:34
0.2% 7 matches


- [27]  from a PlagScan document dated 2018-03-04 07:51
0.0% 6 matches


- [28]  from a PlagScan document dated 2016-03-27 10:59
0.0% 8 matches


- [29]  from a PlagScan document dated 2020-08-27 15:21
0.0% 6 matches


- [30]  Structure of the Mt Isa region from seismic ambient noise tomography
0.2% 5 matches


- [32]  A Feasibility Study on Monitoring Crustal Structure Variations by Direct Comparison of Surface Wave Dispersion Curves from Ambient Seis
0.2% 5 matches


- [36]  www.sciencedirect.com/science/article/abs/pii/S0926985111002308
0.3% 4 matches


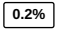

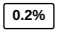

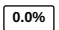

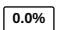

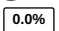

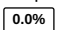

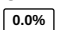

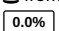


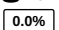

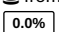

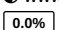

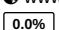

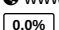

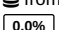


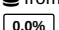

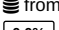




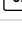

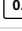
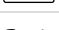
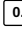
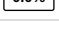
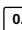
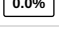

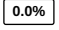

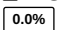

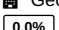

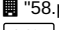


- [40]  from a PlagScan document dated 2021-04-27 08:55
0.0% 6 matches

- [43]  from a PlagScan document dated 2019-02-27 06:48
0.0% 6 matches

- [44]  Shallow magma chamber under the Wudalianchi Volcanic Field unveiled by seismic imaging with dense array
0.0% 5 matches

- [45]  www.researchgate.net/publication/297615791_3D-ambient_noise_Rayleigh_wave_tomography_of_Snaefellsjokull_volcano_Iceland
0.0% 4 matches

- [47]  from a PlagScan document dated 2018-04-02 07:48
0.1% 3 matches

- ✓ [48]  academic.oup.com/gji/article/196/2/1162/580398
 4 matches
-
- ✓ [54]  www.solid-earth-discuss.net/se-2013-57/
 3 matches
-
- ✓ [61]  from a PlagScan document dated 2018-07-08 07:17
 4 matches
-
- ✓ [63]  from a PlagScan document dated 2019-10-06 11:46
 3 matches
-
- ✓ [76]  from a PlagScan document dated 2022-06-27 14:32
 3 matches
-
- ✓ [78]  openfamilystudiesjournal.com/VOLUME/2/PAGE/66/PDF/
 3 matches
-
- ✓ [79]  www.researchgate.net/publication/292159818_Imaging_of_magma_intrusions_beneath_Harrat_Al-Madinah_in_Saudi_Arabia
 2 matches
-
- ✓ [80]  from a PlagScan document dated 2021-07-26 12:01
 2 matches
 1 documents with identical matches
-
- ✓ [82]  from a PlagScan document dated 2020-08-08 13:53
 2 matches
-
- ✓ [83]  from a PlagScan document dated 2018-11-07 16:04
 2 matches
-
- ✓ [84]  www.researchgate.net/publication/332623879_Determinacion_de_la_estructura_de_velocidades_sismicas_de_Corea_del_Sur_a_partir_de
 2 matches
-
- ✓ [85]  www.sciencedirect.com/science/article/abs/pii/S0031018203004620
 3 matches
-
- ✓ [86]  www.sciencedirect.com/science/article/abs/pii/S0012821X20303216
 2 matches
-
- ✓ [90]  from a PlagScan document dated 2021-07-20 03:47
 2 matches
 1 documents with identical matches
-
- ✓ [92]  from a PlagScan document dated 2021-01-20 13:01
 2 matches
-
- ✓ [93]  from a PlagScan document dated 2020-11-17 09:49
 1 matches
-
- ✓ [94]  from a PlagScan document dated 2019-03-30 21:23
 2 matches
-
- ✓ [95]  from a PlagScan document dated 2018-11-07 11:19
 1 matches
-
- ✓ [96]  from a PlagScan document dated 2018-04-22 18:33
 2 matches
-
- ✓ [98]  pdw.hanford.gov/download/55b1f75a-b7d9-4b08-bb42-35ec9ddeb307
 1 matches
-
- ✓ [99]  www.sciencedirect.com/topics/earth-and-planetary-sciences/seismic-tomography
 2 matches
-
- ✓ [100]  from a PlagScan document dated 2021-07-05 12:18
 2 matches
-
- ✓ [101]  "2-تركيبه العيسى.pdf" dated 2021-03-22
 1 matches
-
- ✓ [102]  "Geochemical correlations of oils and organic-rich shales in the Shabwah depression, Yemen.pdf" dated 2019-10-07
 1 matches
-
- ✓ [103]  "58.pdf" dated 2017-03-30
 1 matches
-
- ✓ [104]  from a PlagScan document dated 2022-06-14 06:35
 1 matches
-
- ✓ [105]  from a PlagScan document dated 2022-01-28 12:59
 1 matches

15 pages, 4391 words

PlagLevel: 12.1% selected / 21.6% overall

113 matches from 106 sources, of which 23 are online sources.

Settings

Data policy: *Compare with web sources, Check against organization repository, Check against the Plagiarism Prevention Pool*

Sensitivity: *High*

Bibliography: *Bibliography excluded*

Citation detection: *Highlighting only*

Whitelist: --

AMBIENT NOISE TOMOGRAPHY IN THE UPPER CRUST OF NORTH HARRAT RAHAT, SAUDI ARABIA

Ali K. Abdelfattah^{1,2,✉}, Abdullah Al-amri¹, Hassan Alzahrani¹, Bassam A. Abuamarah¹

¹ Department of Geology & Geophysics, King Saud University, Riyadh 11451, Kingdom of Saudi Arabia

² Department of Seismology, National Research Institute of Astronomy and Geophysics, Egypt

Abstract

We used a continuous dataset of ambient noise to image the crustal structure beneath North Harat Rahat, Saudi Arabia. For this purpose, the technique depends on the Rayleigh-wave group velocity tomography used. The dataset comprises six months of recordings extracted from 12 broadband seismological stations in north Harrat Rahat, Saudi Arabia. Using a cross-correlation technique, the Rayleigh waves have been generated and stacked along the whole time series of the dataset between 1 and 15 s in the period. Dispersion curves representing fundamental mode Rayleigh waves were measured by a multiple filter technique. Dispersion curves for each station pair were inverted to obtain the one-dimensional model of corresponding shear wave velocities. The spatial distribution of shear wave velocities was depicted from the inverted one-dimensional models at 138 nodes and a reliable resolution was spatially resolved using grid cells of 0.2° expanded over both latitude and longitude.

^[1] Results showed two low-velocity zones in the middle and upper crust at depths of 15 km west and shallow 10 km east, respectively, indicating a presence of high conductivity due to upwelling magma flow towards the northeast from plausible deep sources of the Red Sea Rift or Afar plume into the upper crust of the Arabian Shield.

Keywords: Ambient noise, cross-correlation, seismic tomography

^[0] 1. Introduction

The Arabian shield, representing the eastern flank of the Red Sea, is speculated to be characterized by a

✉ correspondence: ali_kamel@yahoo.com & aabdelfattah@ksu.edu.sa

complex geodynamic process due to the active asthenosphere that made the lithosphere enriched in many basaltic volcanic eruptions called Harrats (Fig.1). Tectonically, the Neoproterozoic Arab-Nubian region is adapted to the divergent movement of the Arabian plate concerning the Nubian plate.^[3] Owing to diverse tectonic series, the formation of the NW-SE dikes parallel to the Red Sea, the NE-SW strike-slip faults, and NW normal faults are recognized in the Arabian shield.^[8] Structurally, the regions of Harrats are related to the tectonic rift acting in the Red Sea that might associate with a sequence of Cenozoic bursts, volcanic rocks and ridges. Debayle et al.^[0] (2001) show evidence of an upper-mantle low-velocity material under the Nubian and Arabian lithosphere. Heterogeneities may affect Red sea development. Based on three-dimensional analogue experiments, distinctive morphology was noteworthy in the Red sea due to pre-existing heterogeneities in both crust and mantle (Molnar et al. 2020).^[8] It is well known that basaltic volcanic fields may host between 150 and 300 °C geothermal systems of remains elusive how recent magmatic activities are related to the Red Sea rifting or Afar plume or Jordan plumes.^[8] Recent studies carried out to investigate the fine and gross structure of the lithosphere (Hansen et al. 2013; Koulakov et al, 2015) have not resolved the enigmatic phenomena of magma flow sources and origins of lava fields beneath the basaltic volcanic fields of western Saudi Arabia, indicating a progressively younger flow of magma north toward that may constraint with the bimodal distribution of Konrad et al. (2016).^[0] It suggests that a lateral flow of magma beneath Harrat Rahat comes from the Afar plume and then the active asthenospheric material causes the thinning of the lithosphere in the Arabian Shield.

When few earthquakes are available and inadequate to cover paths from source to receiver well, tomographic techniques depend on using earthquake data are not appropriate for mapping the upper crust with reliable accuracy where intrusions of magma channels or dykes are expected. This problem can be resolved by applying the tomographic technique to the dataset that comprises continuous ambient seismic noise (Shapiro et al., 2005). This technique has been applied on different scales using continuous records of seismic noise that represent a few hours to a few months (Brenquier et al., 2007;

Bensen et al., 2008; Mordret et al., 2013). Theoretically, estimates of Green's function for each station pair can be retrieved from the cross-correlation of continuous ambient noise records, giving signals equivalent to that surface waves recorded at one station and originating from a surface point source acting at other station locations. The retrieval signals from the cross-correlation technique showed spectral amplitudes influenced by the effects of the ambient ground motions and Green's function excitations.

^[30] Using a dataset of twelve seismic monitoring stations collected in the seismic monitoring network established by the Saudi Geological Survey, we implemented the ambient noise tomography approach in this study. The results presented here focus on the propagation of ambient noise within the northwest part of Harrat Rahat, Saudi Arabia.

2. Crustal heterogeneities in Arabian Shield

The high plateaus that represent the western flank of the Red Sea can reach an elevation of 2,000 meters or more in some localities and consist of large Precambrian basement rocks (600-900Ma). These rocks are believed to contain little or no sedimentary rocks. They are considered as rifted continental margins. The eastern flank known as the Arabian shield is considered a Juvenile Neoproterozoic crust showing granite, schist, gneiss, volcanic and sedimentary rocks. Ultramafic and ophiolitic rocks are recognised also in some localities. These uplifted Precambrian rocks are intruded by Cenozoic basalt and intrusive volcanic rocks (Fig.1).^[1] The formation of the Arabian Shield results from the convergence of the continental segments that occurred between 630 to 550 Ma (Stern and Johnson 2010).^[1] The Arabian Shield was tectonically adopted by the divergence of the Arabian and African plates during Cenozoic volcanism, giving rise to the Red Sea rifting. According to existing evidence, the Precambrian rocks of the Arabian Shield underwent many tectonic phases.^[0] Brittle and ductile faults, NW normal faults and dikes, which are known to run parallel to the Red Sea, and N-S to NE strike-slip faults, which are well known in the southern Arabian shield, are among the dominant structures in the

Arabian Shield.

^[0]▶ The continuous regional extension tectonic movement that began 30 Ma ago and is associated with the Cenozoic volcanic activity in the region is what caused the Red Sea rifting. (Coleman et al., 1983). The Precambrian basement is composed of different igneous rocks that are exposed at the surface and have remarkable NW-SE and NE-SW trends. Jonsson (2012) identified some surface faults, the majority of which are parallel to the Red Sea rift and striking in the NW-SE trend, regarded as tensional fractures that are typical normal fault styles. The geologic map also displays the most recent volcanic rock observations imputed to the 10th-century eruption. ^[3]▶ It is believed that hot materials in the upper mantle of the Arabian Shield are responsible for the formation of all Cenozoic volcanic rocks known as Harrats including Harrat Rahat (Camp and Roobol, 1992).

3. Data and methods

3.1 Data and calculation of Green functions

Digital wave recordings were collected from twelve broadband seismic stations that were established by the Saudi Geological Survey (SGS) in north Harrat Rahat. Velocity sensors of Trillium 120 s combined with trillium digitizers represented the main components of all instruments. Locations of seismic stations and ray-path coverages between seismic stations are depicted on a map in Figure 1.

We employed the cross-correlation method, which is often used to cancel out the typical instrumental phase response and enhance the impact of the instrumental amplitude response. To reduce the impacts of earthquakes and non-stationary noise sources near seismic stations, a whitening process was used to reduce amplitude distortion. Higher signal-to-noise ratios are often provided through cross-correlation calculations that were performed between station pairs with longer time-series lengths (Bensen et al., 2008). In this analysis, we used Digital waveform data for continuous recordings that represented six months starting from January 1 to June 2014. The seismic noise records are processed in 46 half-hour portions starting at 00:30 and finishing at 23:30 to enhance the signal-to-noise ratio and

prevent potential data loss due to the start and end times of the original raw data (Cho et al., 2007). To provide a flat amplitude spectrum in the 0.05-5 Hz band tapered to zero in the frequency range 0.02-8 Hz, the half-hour segment spectra are whitened. The phase bias of the instruments is subsequently removed by cross-correlating the whitened traces with corresponding instrumental responses. All 46 half-hour cross-correlation functions were symmetrically calculated and stacked over the aftermentioned frequency band.

To obtain the empirical Green's functions, all-day stacks that are available for each station pair are stacked. Using computer programs in seismology written by Herrmann and Ammon (2004), we adapted some scripts for this procedure. For the Rayleigh wave extractions, Empirical Green's functions were recovered over all conceivable ray paths. Figure 2 illustrates an example of retrieving the empirical Green's function between vertical component recordings.

3.2 Group velocity measurements

A multiple-filter method was used to estimate the dispersion curves of Rayleigh-wave fundamental modes from each retrieved empirical Green's function (Dziewonski et al., 1969; Herrmann, 1973). In order to satisfy the requirement for employing the cross-correlation approach with ambient seismic noise, the dispersion curves of group velocity were measured for station pairs that are at least two wavelengths apart (Brenquier et al., 2007). Only the intelligible dispersion curves were chosen while the distorted ones were disregarded. The multiple filter analysis (MFA) of the vertical components between station pairs produced the group velocities that were displayed in Figure 3 as a variation against their respective periods. On the right of Figure 3, the band pass filtered signal is shown. The band-pass filter with corners at 0.03 and 1 Hz was employed to filter the seismograms after the data trend was eliminated.

Because the dispersion curves are flattened and the signal-to-noise ratios are weakened, it is frequently difficult to explicate contour maps generated by the MFA. Within the period span ranging from 1 to 15

s, the main energy was tapered and we were able to detect the group velocities of the Rayleigh wave. At a central frequency of 0.25Hz, the highest possible number of 138 ray paths was attained. Figure 4 shows examples of dispersion curve measurements along several ray paths.

Using the SURF96 package (Herrmann and Ammon, 2004), the dispersion curves were inverted to produce a one-dimensional velocity model at 138 nodes of each grid to enhance depth resolution.^[36] In order to recover the one-dimensional velocity model from the inversion of Rayleigh wave dispersion curves, the one-dimensional velocity model of Rogger et al. (1999) was used as an initial model.^[32] At selected grid nodes denoted by the interstation distance between each station pair, the velocity structure fitted to the dispersion curves is shown in Figure 5. Additionally, the derived velocity models related to observed and theoretical dispersion curves are displayed in Figure 5.

3.3 Group velocity tomography

We calculated the group velocities of fundamental modes by measuring the travel times over a range of defined periods between 1 and 15 s and the interstation distance between station pairs. After obtaining the dispersion curves that depict the travel path between station pairs, maps of the retrieved Rayleigh-wave group velocities were produced using a non-linear iterative 2-D tomographic method (Rawlinson et al., 2008).

The ray paths between station pairs were simultaneously updated during the inversion processing in order to take into consideration the impact of the ray lengths while theoretical arrival times are calculated. The Fast Matching Method (FMM; Rawlinson and Sambridge 2004a, b) is employed in this inversion approach to representing group velocity tomography of Rayleigh waves. In tectonic and volcanic settings which are characterized by extremely heterogeneities, the FMM depending on a grid Eikonal solution that incorporates implicit wavefront generation was performed in order to obtain stable and reliable solutions for wave propagation.

Half-space velocity is the approximation model used to start the inversion procedure. The only

variable parameter is the S-wave velocity that updates for each layer during the iteration process. The inversion procedure keeps searching for variations in the model's parameters until the group velocity that reflects the best match is found. The tomographic inversion was carried out using a discretized grid of $0.2^\circ \times 0.2^\circ$ cells at each period, which demonstrated an acceptable resolution and stability of the inversion findings. Synthetic checkboard tests were performed to examine the geometrical resolution of ray trajectories depicting between station pairs. For each corresponding period, a constant velocity perturbed by 0.5 km/s from the apparent average group velocity was allocated to each test model. The same scheme and parameters used for the observational arrival times were performed to compute and invert the synthetic arrival times for each station pair. To assess the sensitivity to various size configurations, a range of different grid sizes was examined. The most logical resolution is represented by a grid with cells that are $0.2^\circ \times 0.2^\circ$ in size. The checkboard resolution test for the $0.2^\circ \times 0.2^\circ$ grid size is shown in Figure 6 for the same ray trajectories of the observed Rayleigh waves at the corresponding periods.

^[0] In order to recover the 3-D model of S-wave velocities in the upper crust of Harrat Rahat, an inverted one-dimensional S-wave velocity profile was created for each node in a manner equivalent to Bensen et al. (2009) and Choi et al. (2010). Each 1-D model's velocities at 1 km depth intervals were interpolated using linear interpolation, and all of the nodes were then smoothed using a minimum curvature spline developed by Smith and Wessel (1990). ^[0] To highlight the spatial distribution of the three-dimensional model, slices in figure 7 display lateral and vertical variations in shear wave velocities for corresponding depths of 5, 10, 15, 20, and 25 km.

4. Discussions

The findings obtained from the current investigation demonstrated that the lithosphere under Harrat Rahat is heterogeneous as evidenced by the spatial distribution of three-dimensional velocities.

^[8] The heterogeneity may be attributed to the complexity of the tectonic phases that ranged from the

periods of Precambrian to the active Cenozoic basaltic fields that resulted in the formation of dikes parallel to the Red Sea axial rift, strike-slip faults, normal faults, and Cenozoic volcanisms, characterizing the lithosphere of the Arabian shield.

Two low-velocity zones that are depicted by the tomographic images in the upper crust of North Harrat Rahat are the most interesting sign in the tomographic pictures derived from this study. The deeper zone is dominant towards the west and the shallower zone is located towards the east. Along with previous studies' hypotheses of Camp and Roobol (1992), Bensen et al. (2009), Choi et al. (2009), Chang and van der Lee (2011), Chang et al. (2011), and Chang et al. (2015), we propose that the simplest explanation for the tomographic images is the existence of magma upwelling from plausible deep sources such as the Red Sea Rifting and Afar plume into the lithosphere of Harrat Rahat. According to this scenario, the spatial distribution of Cenozoic basaltic fields in enriched patterns over the Arabian Shield emphasises that the explanation of magma upwelling is plausible.

^[0] The origin of the Cenozoic basaltic fields that enriched along the Arabian Shield is still poorly understood although several studies investigated the velocity structures beneath the Shield. Recently, the ambiguous spatial connection between the Cenozoic volcano in West Saudi Arabia, the Rift Axis of the Red Sea, and deeper low-share wave velocity region of unknown source origin are revealed by regional seismic tomography (Chang et al., 2011). Several models are suggested for the active asthenosphere of the Arabian shield. ^[0] A local mantle plume below the Arabian lithosphere has been proposed by Camp and Roobol (1992). ^[0] Chang and van der Lee (2011) postulated a lateral mantle flow from the Afar plume and possibly from the Jordan hotspot.

^[0] Despite various studies that investigated the velocity structures under the Arabian Shield, the formation of the Cenozoic basaltic fields that developed along the Shield is still not well understood and from which sources ascended. ^[0] A questionable relationship between the Rift Axis of the Red Sea, the spatial distribution of the Cenozoic volcano in the Arabia Shield, and a deeper low-share wave velocity zone with an unexplained source origin have recently been revealed using regional seismic

tomography (Chang et al., 2011). For the Arabian shield's active asthenosphere, many models are suggested. Camp and Roobol (1992) have postulated that a local mantle plume exists under the Arabian lithosphere.^{[0]▶} A lateral mantle flow from the Afar plume and maybe from the Jordan hotspot was proposed by Chang and van der Lee (2011).

On the regional scale, the study of Chang et al.^{[11]▶} (2011) directed low shear velocities beneath the southern Red Sea and the western Arabian plate that may support the idea of lateral mantle flow from the Afar. On the global scale, the model deduced by Chang et al.^{[0]▶} (2015) depicted a low-velocity region that extends from the lower mantle beneath South Africa to the upper mantle beneath the Afar with no clear connection to the low-velocity zones beneath the Arabian Shield.^{[1]▶} Recent studies revealed that the velocity structures beneath Cenozoic basaltic fields in the Arabian Shield are characterized by low-velocity zones that are presumably related to lava fields that ahead progressively younger northwards of unknown exact origin.^{[0]▶} Chang et al (2011) pointed out on a regional scale that low shear velocities are distributed under the Arabian Shield and the southern Red Sea, which may support the theory of lateral mantle flow from the Afar plume. The model developed by Chang et al.^{[0]▶} (2015) showed a low-velocity zone on a global scale that moves from the lower mantle beneath South Africa to the upper mantle beneath the Afar with no coherent explanation for the low-velocity zones beneath the Arabian Shield. According to recent investigations, the velocity structures under the Cenozoic basaltic fields in Arabian Shield are distinguished by low-velocity zones that are probably connected to lava fields that extend farther northward with no exact origin suggested.

The magma flow under the Arabian Shield has several possible explanations.^{[0]▶} It is speculated that the Red Sea rift or the Afar plume is thought to be the source of a lateral flow of magma that entered the upper crust of Harrat Rahat (Konrad et al., 2016; Mai et al., 2019). According to the isotopic ratios of helium from lava flows and mantle xenoliths that were collected from distinct harrats in Saudi Arabia and Yemen, a bimodal distribution of Harrat Rahat is suggested by Konrad et al. (2016) that indicates the lateral magma flow moves from the Afar plume into the Arabian Shield.^{[0]▶}

The upper lithosphere of the Arabian shield may be experienced a mixing of morphospheric materials as a result of the effect of thermal erosion and convective instability. Accordingly, the magma plume will be confined to the lava mixture in Harat Rahat.^[3] In addition, the Arabian shield and the Red Sea coastline exhibit a remarkable transition from oceanic crust to continental crust, abruptly, with evidence of crust thickening as we move westward to the eastern coastlines of the Red Sea (Tang et al., 2016). Cenozoic volcanic structures of the Arabian lithosphere have been hypothesized to be recognized by low shear velocities and high temperatures, supporting thermal conductivity due to the magma flow ascending from the Afar plume into the Arabian shield through fractures in the crust that may give rise to local magma diapirs occurred in the Arabian lithosphere (Mai et al., 2019).

To this end, the upwelling of magma plume materials that occur below Harrat Rahat remains an open question that requires a detailed mapping of the border between lithosphere and asthenosphere, as well as the lateral flow of active asthenosphere, which should be modelled beneath the Arabian Shield (e.g., Faccenna et al. 2013).^[0] High-resolution data that can give rise to high-resolution tomographic images for deeper depths and cover more wide area is required to provide a clear scenario for the originality of plausible sources and propagation path of magma flow in the crust and upper mantle beneath Harrat Rahat.

^[0]To this end, a comprehensive mapping of the interface between the lithosphere and asthenosphere as well as the lateral flow of active asthenosphere, which should be modelled beneath the Arabian Shield, are required to address an open question of the plausible upwelling of magma plume materials that occur beneath Harrat Rahat (e.g., Faccenna et al. 2013).^[0] To provide an understandable scenario for the originality of the potential sources and propagation channels of magma flow in the crust and upper mantle under Harrat Rahat, high-resolution data that can enhance the production of high-resolution tomographic images at deeper depths and larger scales is essential.

5. Conclusions

The present study focuses mainly on the multiple-analysis stages to explore the crustal structure under Harrat Rahat using continuous data on ambient noise. A total number of 138 nodes, depicted at the interstation distance, between each station pair were represented by Rayleigh wave dispersion curves of fundamental modes that were generated using the cross-correlation approach and stacked for six months of continuous data. An iterative technique was used to retrieve the one-dimensional velocity model at each node. Finally, the three-dimensional structure under Harrat Rahat was depicted using one-dimensional velocity models obtained from this study. Within the upper crust, two low-velocity anomalies were depicted.^[0] The shallow anomaly was found at a depth of 5–10 km towards the west of the studied area and the other low-velocity anomaly over a depth of more than 15 km was located.^[0] The results obtained from this study support a magma flow that corresponds to the earlier suggestion of magma upwelling from the deep plausible magma sources of the Red Sea Rift and the Afar plume into the lithosphere of Harrat Rahat.^[0] It implies a magma flow coming from the depth of the source westward into the upper crust of Harrat Rahat in the east.

Acknowledgements

This research was supported by Researchers Supporting Project number (RSP2022R425), King Saud University, Riyadh, Saudi Arabia.

References

- Bensen GD, Ritzwoller MH, Barmin MP, Levshin AL, Lin F, Moschetti MP, Shapiro NM, Yang Y (2008) Processing seismic ambient noise data to obtain reliable broad-band surface wave dispersion measurements. *Geophys J Int* 169(3): 1239–1260.
- Bensen GD, Ritzwoller MH, Shapiro NM (2009) Broadband ambient noise surface wave tomography across the United States. *J Geophys Res* 113: B05306. doi:200810.1029/2007JB005248

- Brenguier F, Shapiro NM, Campillo M, Nercessian A, Ferrazzini V (2007) 3D surface wave tomography of the Piton de la Fournaise volcano using seismic noise correlations. *Geophys. Res. Lett.* 34: L02305.
- Camp V, Roobol M (1992) Upwelling Asthenosphere Beneath Western Arabian and Its Regional Implication. *Journal of Geophysical Research*, 97, 15255–15271.
- Chang SJ, Van der Lee S (2011) Mantle plumes and associated flow beneath Arabia and East Africa. *Earth Planet. Sci. Lett.* 302 (3), 448–454.
- Chang SJ, Merino M, Van der Lee S, Stein S, Stein CA (2011) Mantle flow beneath Arabia offset from the opening Red Sea. *Geophys. Res. Lett.* 38 (4).
- Chang SJ, Ferreira AM, Ritsema J, Heijst HJ, Woodhouse JH (2015) Joint inversion for global isotropic and radially anisotropic mantle structure including crustal thickness perturbations. *J. Geophys. Res. Solid Earth*, 120, 4278–4300
- Cho, K. H., R. B. Herrmann, C. J. Ammon, and K. Lee (2007), Imaging the upper crust of the Korean Peninsula by surfacewave tomography, *Bull. Seismol. Soc. Am.*, 97, 198–207.
- Choi J, Kang T-S, Baag Ch-E (2009) Three-dimensional surface wave tomography for the upper crustal velocity structure of southern Korea using seismic noise correlations. *Geosciences Journal* 13(4):423–432.
- Coleman RG, Gregory RT, Brown GF (1983) Cenozoic volcanic rocks of Saudi Arabia. USGS Open-File Report 83–788, 82 pp.
- Debayle E, L ev eque J, Cara M (2001) Seismic evidence for a deeply rooted low-velocity anomaly in the upper mantle beneath the northeastern Afro/Arabian continent. *Earth Planet. Sci. Lett.*, 193(3), 423–436.
- Dziewonski A, Bloch S, Landisman M (1969) A technique for the analysis of transient seismic signals. *Bull Seismol Soc Am* 59:427–444

- Faccenna C, Becker Th, Jolivet L, Keskin M (2013) Mantle convection in the Middle East: Reconciling Afar upwelling, Arabia indentation and Aegean trench rollback. *Earth and Planetary Science Letters* 375: 254–269.
- Hansen SE, Deshon HR, Moore-Driskell MM, AlAmri AM (2013) Investigating the P wave velocity structure beneath Harrat Lunayyir, northwestern Saudi Arabia, using double-difference tomography and earthquakes from the 2009 seismic swarm. *J Geophys Res Solid Earth* 118(9):4814–4826.
- Herrmann RB, Ammon CJ (2004) Computer programs in seismology. Manual of the Generic Seismic Application Coding (GSAC). Saint Louis University (Version 3.30)
- Herrmann R (1973) Some aspects of band-pass filtering of surface waves. *Bull Seismol Soc Am* 63(2):663
- Jónsson S (2012) Tensile rock mass strength estimated using InSAR. *Geophys Res Lett.* <https://doi.org/10.1029/2012GL053309>
- Konrad K, Graham DW, Thornber CR, Duncan RA, Kent AJ, Al-Amri AM (2016) Asthenosphere–lithosphere interactions in Western Saudi Arabia: Inferences from $^3\text{He}/^4\text{He}$ in xenoliths and lava flows from Harrat Hutaymah. *Lithos* 248: 339–352, doi:10.1016/j.lithos.2016.01.031.
- Koulakov I, El Khrepy S, Al-Arifi N, Kuznetsov P, Kasatkina E (2015) Structural cause of a missed eruption in the Harrat Lunayyir basaltic field (Saudi Arabia) in 2009. *Geology* 43(5): 395–398, doi:10.1130/G36271.1.
- Mai PM, Julia J, Tang Z (2019) Crustal and Upper-Mantle Structure Beneath Saudi Arabia from Receiver Functions and Surface Wave Analysis. *Geological Setting, Palaeoenvironment and Archaeology of the Red Sea*, 307–322.
- Molnar N, Cruden A, Betts P (2020) The role of inherited crustal and lithospheric architecture during the evolution of the Red Sea: Insights from three dimensional analogue experiments. *Earth Planet. Sci. Lett.* 544: 116377.

- Mordret A, Shapiro NM, Singh S (2013) Seismic noise-based time-lapse monitoring of the Valhall overburden. *Geophys. Res. Lett.* 41: 4945–4952, doi:10.1002/2014GL060602.
- Rawlinson N, Sambridge M (2004a) Wave front evolution in strongly heterogeneous layered media using the fast marching method. *Geophysical Journal International* 156: 631–647.
- Rawlinson N, Sambridge M (2004b) Multiple reflection and transmission phases in complex layered media using a multistage fast marching method. *Geophysics* 69: 1338–1350.
- Rawlinson N, Sambridge M, Saygin E (2008) A dynamic objective function technique for generating multiple solution models in seismic tomography. *Geophysical Journal International* 174: 295–308.
- Rodgers A, Walter W, Mellors R, Al-Amri A, Zhang Y (1999) Lithospheric structure of the Arabian shield and platform from complete regional waveform modelling and surface wave group velocities. *Geophysical Journal International* 138:871–878
- Shapiro NM, Campillo M, Stehly L, Ritzwoller MH (2005) High-resolution surface wave tomography from ambient seismic noise. *Science* 307: 1615–1618.
- Smith WHF, Wessel P (1990) Gridding with Continuous Curvature Splines in Tension. *Geophysics* 55(3):293–305, doi:10.1190/1.1442837
- Stern RJ, Johnson PR (2010) Continental lithosphere of the Arabian Plate: a geologic, petrologic and geophysical synthesis. *Earth Sci Rev* 101:29–67.

